



Pulse thermography applied on a complex structure sample: comparison and analysis of numerical and experimental results

Mirela Susa, Clemente Ibarra-Castanedo, Xavier Maldague and Abelhakim Bendada
Université Laval
Québec (QC), G1K 7P4, Canada
Tel.: +1 418 656 2131 (4876)
Telefax: +1 418 656 3159
msusa@gel.ulaval.ca

Srecko Svaic, Ivanka Boras
Faculty of Mechanical Engineering and Naval Architecture
Zagreb, 10 000, Croatia

Abstract

The purpose of this work was to determine the possibility of modeling complex structure samples inspected by infrared thermography, as well as the possibility of identifying the defect characteristics, in particular the defect type, using the results obtained. The paper presents the analysis of results obtained by pulse thermography experiments on a complex structure sample containing defects of different types and sizes located at different depths. The sample tested was made of two different types of honeycomb panel with inserted defects of specified size, position and type. The sequence of thermograms obtained by experiment was used to extract the surface temperature evolution curves above the defective and non-defective sample areas. These evolution curves were used for comparison of the experimental results and results obtained by numerical modeling. Furthermore, thermal contrast evolution curves were used to analyze the differences in results obtained experimentally and through modeling.

For purposes of finite element analysis, a model of the tested sample was made so that the finite element method (FEM) could be used to solve the problem of transient heat transfer occurring in experimental conditions. Unknown parameters of the numerical model (such as power density of the heat source used in experiment, convective heat transfer coefficients and sample surface emissivity) were adjusted to obtain results of numerical simulation as close as possible to those obtained experimentally. In a similar way, the surface temperature decay curves were extracted from the numerical model results. Similarities and differences in the results obtained were analyzed and discussed. Possibilities for improving the results and further research activities are proposed.

Keywords: NDT, Infrared Thermography, Pulse Thermography, Finite Element Method, Heat Transfer

1. Introduction

Like many other fields of application, infrared thermography has benefited from rapid technical development of imaging systems. The increased performance of infrared cameras when spatial and temperature resolution are considered has led to defect detection improvements. Despite the fact that the defect detection efficiency increased, defect characterization procedures are still a wide area of research. One of the approaches used for years now, especially when pulse experimental procedure is concerned, consisted in determining the defect characteristics using different mathematical models as a means of predicting the defect behavior within the sample subject to experimental conditions. Since the physical nature of the heat transfer occurring during the experiment was well known to be governed by the differential equation of the transient heat transfer, the main problem of the approach was finding the solution to this equation that would permit the comparison of the experimentally and theoretically obtained results. Simplifications were used in many cases that considered the heat transfer only in one direction (1D heat transfer models) that were then solved analytically [1]. Authors also used iterative methods to find solutions to the 1-D problem defined analytically [2]. In addition, most of them neglected heat losses from the surface in order to further simplify the solution [3], [4], [5]. Some authors expanded analytical solutions of 1-D models onto 2-D models using thermal quadrupoles and Laplace transformations [6], [7]. The analytical perturbation method for the solution in 3-D has also been proposed [8]. On the other hand, a numerical method based on finite differences was used in cases where the symmetry was taken as a constraint: in such a way a 2D model of heat transfer was obtained that was equal to a 3D heat transfer model in cylindrical coordinates and it was solved using finite differences [9], [10]. Control volumes were used in [11] for the 2-D heat transfer problem and another numerical solution was proposed in [12] for corrosion evaluation using 3-D heat transfer conditions. Finally the use of FEM was reported as an interesting tool for modeling pulse experiment heat transfer conditions in 3-D in [13] and [14].

This work concentrates on modeling of complex structure samples in an attempt to verify the possibilities of using FEM for purposes of solution retrieval for corresponding established mathematical model in case of more complex samples with multiple different defect types present.

2. Experiment

In order to obtain the data needed to develop a numerical model evaluation, a pulse experiment was performed on a complex composite structure sample with inserted defects. Sample description as well as the experimental set-up description is given next.

2.1 Sample tested

The sample under inspection was a calibration plate made of two different density honeycomb panels. The honeycomb core was placed between two layers of carbon fiber reinforced plastics (CFRP) with a foam adhesive layer between them of specified type and thickness. Defects of different sizes and types were inserted at different locations within the sample so that two sample halves with two different densities of honeycomb core were symmetrical with respect to the location of the defects. Figure 1 shows the

sample with defects. As can be seen, three different sized TEFLON defects inserted within the upper graphite epoxy layer represented the first type of defect. The second defect type was represented by two different sized TEFLON inserts placed between the adhesive and the honeycomb core. Extra foam adhesive was applied in regions of specified dimensions to account for the third defect type. Finally, the crushed core defect represents the fourth type of defect that could be found in the sample with the honeycomb crushed in the specified region just below the adhesive foam layer.

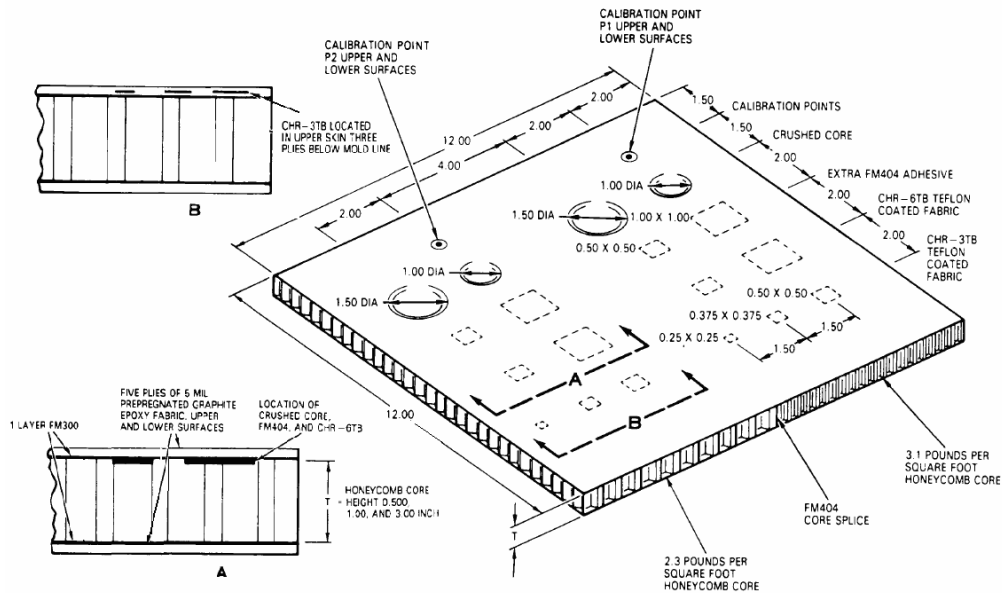


Figure 1 Sample plate drawing with specified type, size and defect position

2.2 Experimental set-up

The experimental set-up can be seen in Figure 2. The experiment was conducted in a reflection mode since it was judged that the sample was too thick for the transmission mode to be successfully employed. Two high power (6.4 kJ), low duration Balcar FX 60



Figure 2 Experimental set-up

flash lamps were used as excitation sources. The pulse duration was 10 ms. Acquisitions were made at frequency of 42.43 fps so that with a maximum number of images acquired, sufficient time duration of the experiment could be captured. An infrared 14 bits ThermaCAM TM Phoenix® camera from FLIR Systems, InSb 640x512 FPA, with Stirling closed cycle cooler operating in the 3-5 nm range was used.

3. Numerical modelling

Solving the transient heat transfer equation provides the theoretical results for temperature evolution of the sample subject to a pulse experiment as in the case considered here. The finite element method is a powerful numerical tool that enables the solution of complex nonlinear, nonsymmetrical mathematical problems governed by partial differential equations such as the one of heat transfer by conduction, convection and radiation with temperature dependant thermal properties of materials involved. In order to solve the given differential equation, model geometry corresponding to the tested sample was defined and its calculation domain divided into finite elements that represent base elements on which the equation solutions are found. The numerical modeling was performed using the software COMSOL 3.2 from Comsol, Inc. The mathematical model used as well as the model geometry and mesh are presented next.

3.1 Mathematical model used

For the problem under consideration 3D heat transfer was taken into account. The differential equation to be solved on the model domain yields:

$$\rho c_p \frac{\partial T}{\partial t} - \nabla \cdot (k \nabla T) = 0 \dots\dots\dots(1)$$

The corresponding initial (2) and boundary conditions included heat transfer by convection and radiation from the object surfaces (3) as well as the heat source applied on the front surface during the first 10ms of the experiment (4). These conditions yielded the following:

$$T(x, y, z, t = 0) = T_{amb} \dots\dots\dots(2)$$

$$\mathbf{n} \cdot (k \nabla T) = h_{conv} (T_{amb} - T) + C (T_{amb}^4 - T^4) \dots\dots\dots(3)$$

$$\mathbf{n} \cdot (k \nabla T) = q_0 + h_{conv} (T_{amb} - T) + C (T_{amb}^4 - T^4) \dots\dots\dots(4)$$

Where T is temperature, T_{amb} is ambient temperature, x, y, z are the space coordinates, ρ is density, $C = \varepsilon_0 \varepsilon_r$ is sample surface emissivity, k is the material heat conductivity, h_{conv} is the convective heat transfer coefficient, c_p is the material heat capacity and t is time.

3.2 Geometry and meshing

The model geometry was defined to correspond to the sample tested. All of the dimensions used in the model were taken from the plate specifications. The defect size

and disposition respect the specifications as well. In the case of the defect type named “crushed core” where no specification was available with respect to the defect thickness, 1 mm was taken as the assumed realistic value that could be expected.

The unstructured mesh used consisted of tetrahedral elements. An adjustment of the mesh parameters permitted a different degree of mesh refinement in regions where larger temperature gradients were expected. In addition, model geometry scaling was used which enabled the large differences in plate dimension proportions to be taken into account so that sufficient mesh refinement was also achieved in the model direction corresponding to plate thickness, much smaller than the two other plate dimensions. Both the model geometry as well as the meshed model used can be seen in Figure 3.

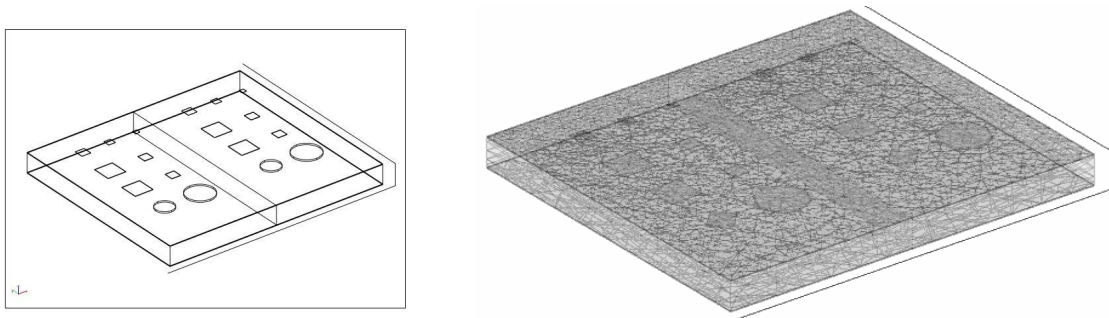


Figure 3 Sample plate drawing with specified type, size and defect position

3.3 Model parameters

Material properties that were used in the model were either taken from literature or values specified by producers were used. In the case of CFRP, the difference in thermal properties with respect to the fiber layout was included into the model. Furthermore, for materials with significantly temperature dependant properties, this dependence was also taken into account. Honeycomb properties were determined in a specific way so as to represent the mean value of the materials of which the honeycomb is composed. For that purpose the honeycomb density provided by the manufacturer was used to determine air and aluminum proportions in each of the two honeycomb types. These proportions were then used to obtain the average properties of two different honeycombs that the sample is composed. The value of the sample surface emissivity coefficient that was used in the model was confirmed by comparing the value of the temperature measured by contact thermometer and the one measured by camera. In addition, the ambient temperature measured in the room was used in the numerical model both as a boundary and an initial condition since it was assumed that the plate was in equilibrium with the environment and therefore at room temperature before the experiment started. Convective heat transfer coefficients used in the model correspond to values recommended in literature for natural convection in still air environment. The density of the heat flux delivered by the heat source, as well as its shape was adjusted so that the numerical results fit as much as possible with the experimental ones.

4. Results and discussion

Both experimental and numerical results for different defect types will be shown next.

4.1 Thermograms and surface temperature distribution obtained numerically

Figure 4 and Figure 5 present two pairs of corresponding sample surface temperature distributions obtained experimentally and from numerical model. Temperature scales are adjusted so that the maximal contrast is obtained for experimental images in order to enhance the visibility of defects. The range of temperatures for the corresponding surface temperature distribution on numerically obtained results was adjusted to correspond to the experimental data temperature scale so that the images can be directly compared. Several observations can be made from the thermograms. First, when earlier thermograms are taken into account, the influence of the honeycomb structure on the surface temperature distribution is noticeable, and thus the honeycomb cells can clearly be distinguished on the images. On the other hand, since in the numerical model the structure is only taken into account via equivalent thermal properties as described earlier, the structure existing inside the panel cannot be reflected in the surface temperature distribution obtained using the model. At the same time, the exact location

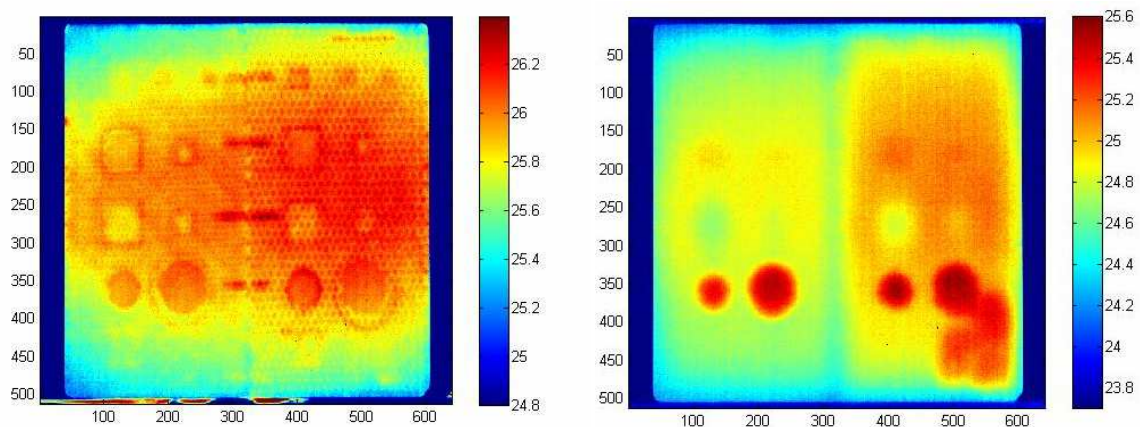


Figure 4 Thermograms obtained from pulse experiment on a sample, left - at $t=2s$ and right - at $t = 20s$ after the heat pulse has been applied

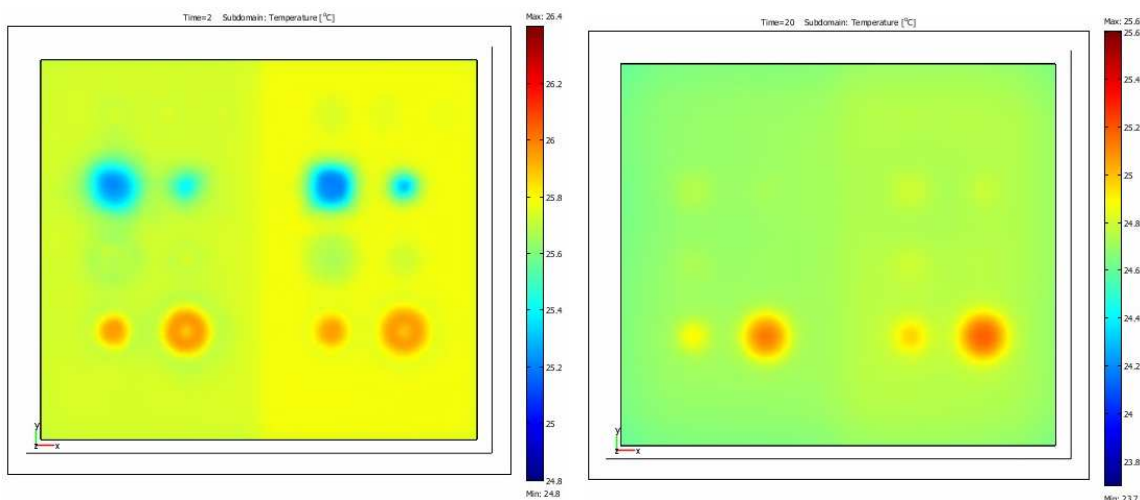


Figure 5 Surface temperature distribution as obtained by numerical simulation corresponding to $t=2s$ (left) and $t = 20s$ (right) after the heat pulse has been applied

of the points representing defective and non-defective areas in the case of experimental data should be chosen carefully because the ‘thermal print’ of the structure will significantly influence the extracted temperature decay curves during the time when the honeycomb structure is visible on the surface. Moreover, it can clearly be seen that rather highly non-uniform heating was present in the experiment. In fact, looking at the early thermograms, it was concluded that heating was stronger towards the center of the plate in a horizontal sense and a bit stronger on the right-hand side of the plate. Still, the fact that the right-hand side of the plate was slower to cool down with respect to the left-hand side is also partly due to the thermal properties of the denser right-hand honeycomb structure. This effect can clearly be seen on results obtained numerically, though not so noticeable mostly due to the fact that in the model uniform heating over the whole surface was applied.

4.2 Time evolution of the temperature decay curves

Figures 6 and 7 represent the temperature decay curves for defective and non-defective areas both obtained experimentally and numerically. In Figure 6 results for the defect type ‘crushed core’ are depicted. The larger difference in behaviour of the defective area curve is partly due to non-uniform heating and partly to the fact that no exact specification was available on the thickness of the defect. On the other hand, Figure 7 shows the results obtained for the defect type ‘core unbound’. The overall difference in temperature levels of the experimental and numerical results is again due to non-uniform heating, but despite certain differences, it can generally be concluded that the decay curves exhibit relatively similar behaviour.

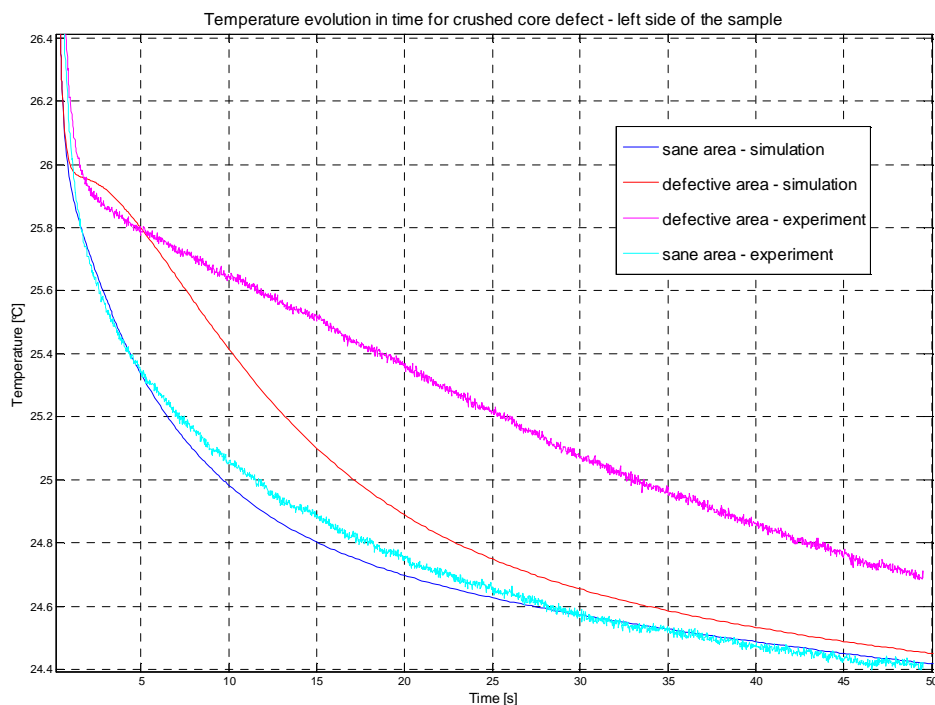


Figure 6 Surface temperature decay curves above the defective and non-defective area, experimental and numerical results; ‘crushed core’ defect; left side of the plate

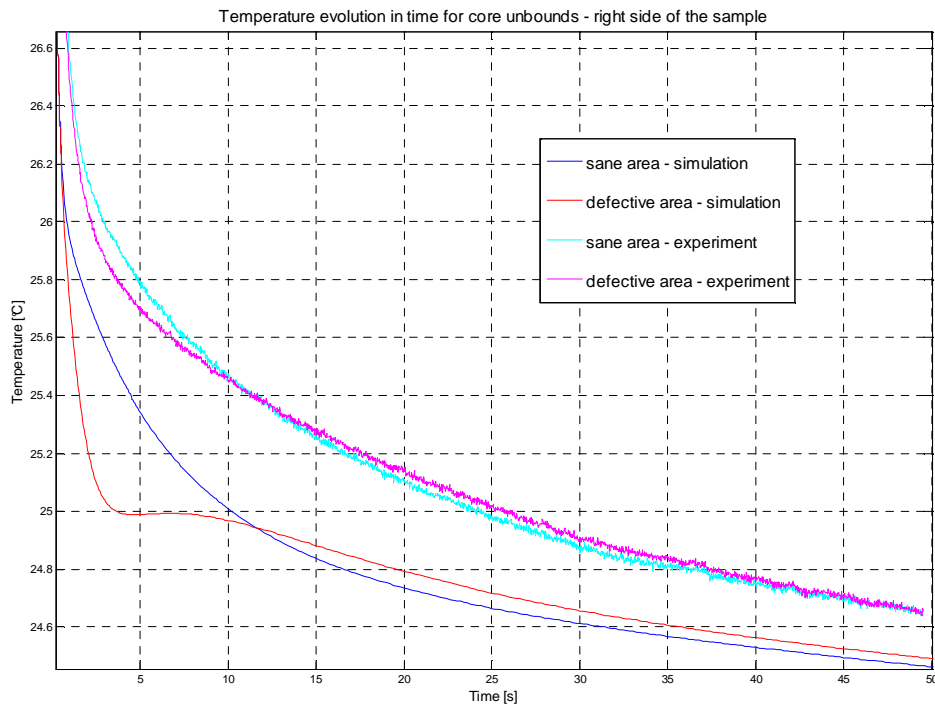


Figure 7 Surface temperature decay curves above the defective and non-defective area, experimental and numerical results, ‘core unbound’ defect, right side of the plate

4.3 Thermal contrast evolution in time

Evolutions of the thermal contrast obtained experimentally and through modeling for each of the four different defect types and two different defect sizes are presented in Figures 8-11. The first two figures (8 and 9) are obtained for defects imbedded in the left-hand side of the panel, while the last two (10 and 11) show the behaviour of the defects on the right-hand-side of the plate. It can be concluded that results of the modeling for defects of type ‘crushed core’ and ‘core unbound’ correspond relatively well to the experimental data. More or less the same conclusion can be applied in the case of the ‘delaminations’ defects, although after just a few seconds following the heat pulse, the thermal contrast obtained was so small that the defects were barely visible, both in case of experiment and simulation. On the contrary, in the case of the ‘extra adhesive’ defect, the behavior of the defect as obtained from experimental data shows no correspondence to the behaviour obtained by modelling. Comparing the results obtained by pulse thermography with those obtained by other methods, it was concluded that the defect does not behave as expected when its simulation thermal properties are considered. This fact raised doubt in accuracy of the data with respect to the thermal properties of the adhesive that was used to simulate defects. These properties were taken according to specifications given with the plate but they can vary widely depending on the final condition of the adhesive mass once applied to the plate.

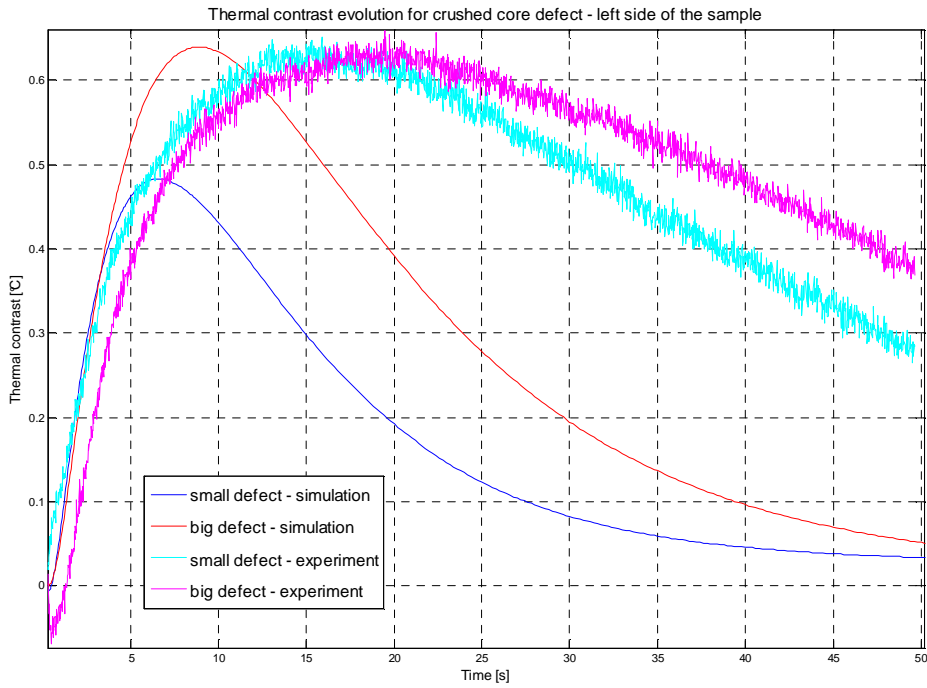


Figure 8 Thermal contrast evolution in time, experimental and numerical results; ‘crushed core’ defect; left side of the plate

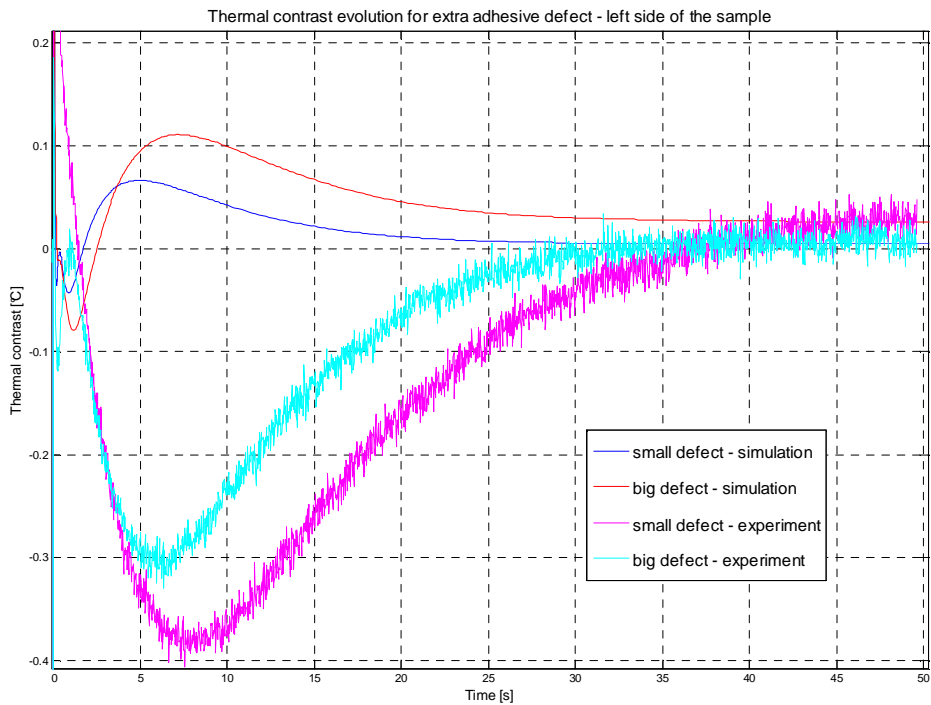


Figure 9 Thermal contrast evolution in time, experimental and numerical results; ‘extra adhesive’ defect; left side of the plate

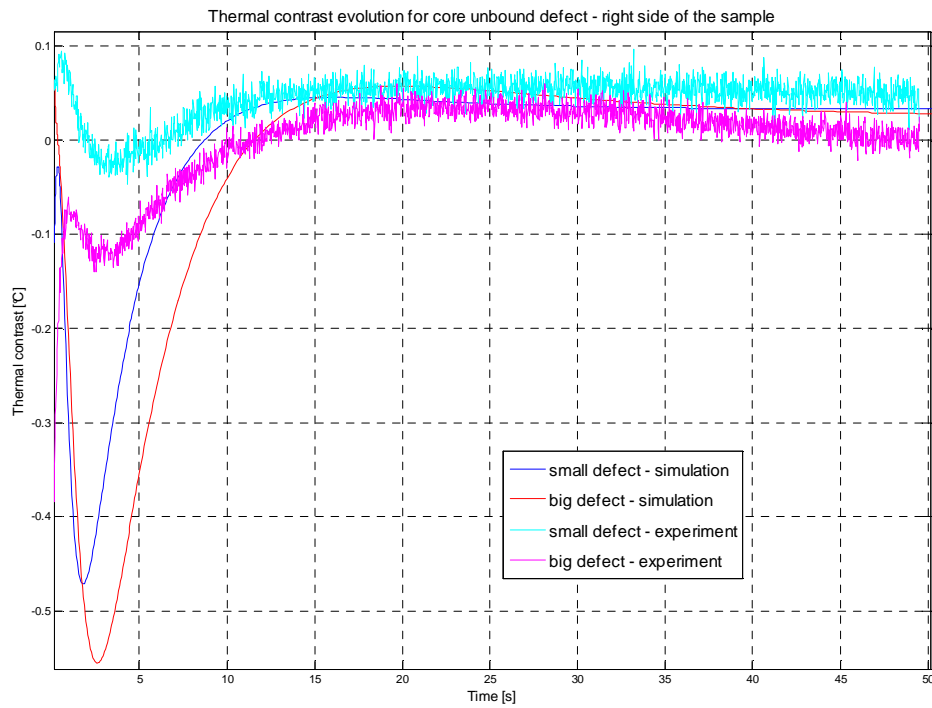


Figure 10 Thermal contrast evolution in time, experimental and numerical results, 'core unbound' defect, right side of the plate

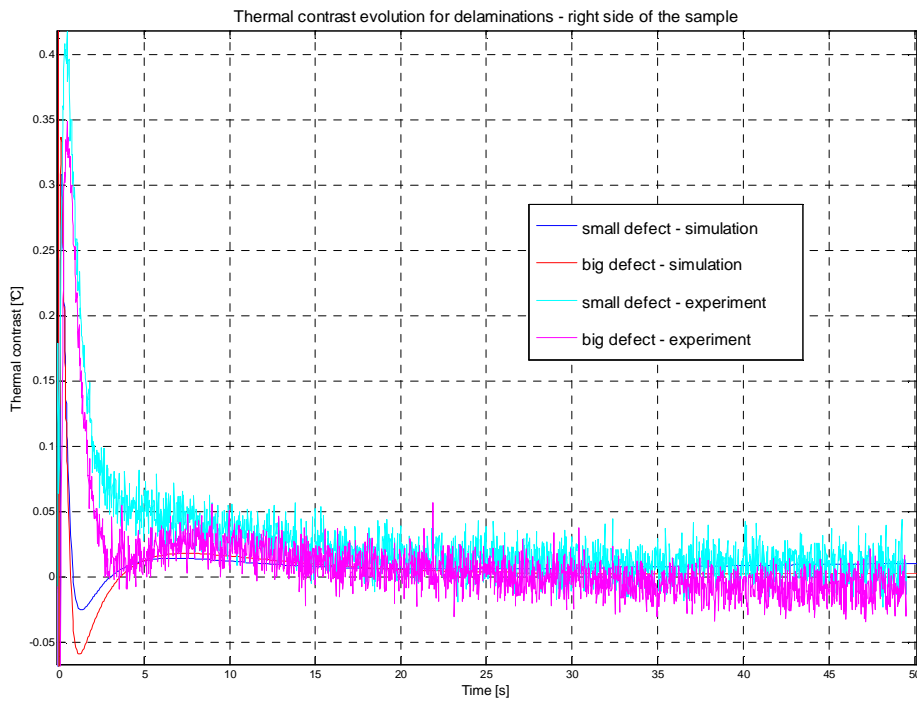


Figure 11 Thermal contrast evolution in time, experimental and numerical results, 'delaminations' defect, right side of the plate

Finally, to illustrate the impact of the non-uniform heating on the experimental results, as well as to point out difficulties that this causes for obtaining experimental data that can truly be comparable to the numerical results, Figure 12 gives the thermal contrast curves for defect type ‘crushed core’ located in the left-hand part of the plate. Data depicted in cyan and green represent the thermal contrast obtained experimentally for the smaller of the two defects. The only difference is in the choice of the reference sane area points. In general, for all of the defects, the non-defective area has been chosen at the same distance from the center of each defect and from the defect center horizontally in the direction opposite from to plate centre. The distance corresponded to half the distance between the centers of the two same defect types. The same was done to obtain the thermal contrast depicted in cyan. The result (thermal contrasts of comparable maximal value for two defects of different sizes) is rather surprising if non-uniform heating is not taken into account. Therefore, in order to obtain the thermal contrast depicted in green, the same reference points were taken for both defects, those in the middle of the defects. Clearly, the smaller defect now shows a lower maximal thermal contrast and thus, the conclusion can be drawn that nonuniform heating has an important impact on the extracted data quality.

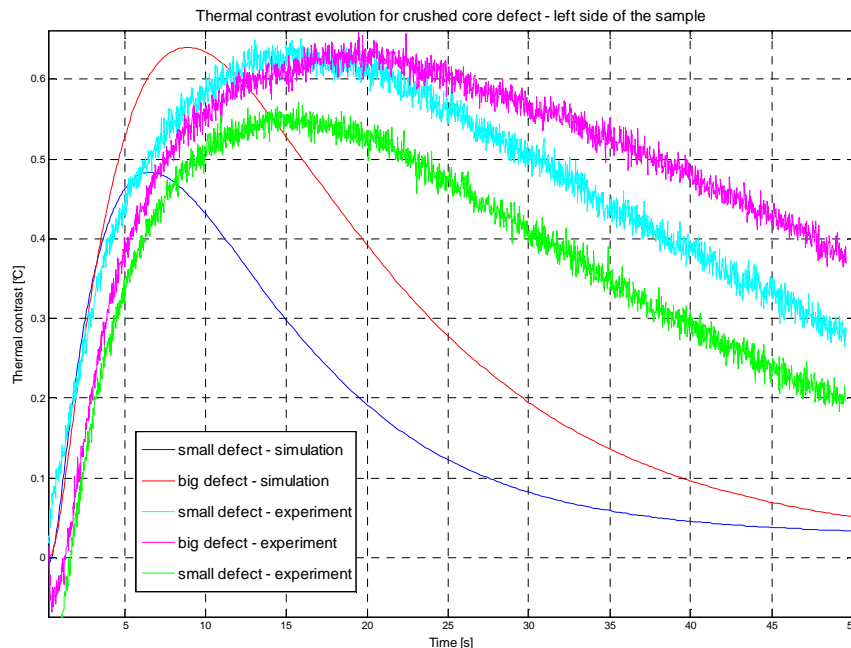


Figure 12 Thermal contrast evolution in time – influence of non-uniform heating, experimental and numerical results; ‘crushed core’ defect; right side of the plate

5. Conclusions and further work

The results obtained thus far in modeling complex composite structures with different defects present have been encouraging. It has been proven that different types of defects have significantly different thermal responses when imbedded in the same structure. Therefore research concerning the possible identification of the defect type by analyzing these specific differences in temperature decay and thermal contrast curves is under way. Non-uniform heating clearly represents one of the main obstacles for easier comparison of the experimental and numerical results needed for numerical model

validation. Since the quantity of the heat delivered to the sample surface directly influences the temperature decay curves and in addition the resulting thermal contrast, a way to overcome this drawback will be examined next. Since it is not possible to eliminate the non-uniformity in heating, a means of taking this experimental condition into account will be considered as the continuation of this work.

Acknowledgements

Support of NSERC, Canadian Foundation of Innovation and Canada Research Chairs (MiViM) as well as the support of Ministry of Science, Education and Sports of Republic Croatia are acknowledged.

References

1. Ph M Delpéch, J C Krapez, D L Balageas, 'Thermal defectometry using the temperature decay method', Proc. of QIRT 94, pp 220-225, August 1994.
2. Ph M Delpéch et al.: 'Time-resolved pulsed stimulated infrared thermography applied to carbon/carbon non destructive evaluation', Proc. of QIRT 92, pp 201-206, July 1992.
3. P Cielo, X Maldague, A A Déom, R Lewak, 'Nondestructive Evaluation of Industrial Materials and Structures ', Materials evaluation, Vol. 45.,pp 452-460, April 1987.
4. D L Balageas, A A Déom, D M Boscher, 'Characterization and Nondestructive Testing of Carbon-Epoxy Composites by a Pulsed Photothermal Method', Materials evaluation, Vol. 45.,pp 452-460, April 1987.
5. D P Almond and S K Lau, 'Defect sizing by transient thermography I: an analytical treatment', J. Phys. D: Appl. Phys., Vol 27, pp 1063-1069, 1994.
6. D Maillet et al., 'Non-destructive thermal evaluation of delaminations in a laminate: Part I – Identification by measurement of thermal contrast', Composites Science and Technology, Vol 47, pp 137-153, 1993.
7. D Maillet et al., 'Non-destructive thermal evaluation of delaminations in a laminate: Part II– The experimental Laplace transforms method', Composites Science and Technology, Vol 47, pp 155-172, 1993.
8. A Bendada, F Erchiqui, M Lamontagne, 'Pulsed thermography in the evaluation of an aircraft composite using 3D thermal quadrupoles and mathematical perturbations', Inverse problems, Vol 21, pp 857-877, 2005.
9. D P Almond, M B Saintey, S K Lau, 'Edge-effects and defect sizing by transient thermography', Proc. of QIRT 94, pp 247-252, August 1994.
10. M B Saintey and D P Almond, 'Defect sizing by transient thermography II: a numerical treatment', J. Phys. D: Appl. Phys., Vol 28, pp 2539-2546, 1995.
11. J C Krapez et al., 'Time-resolved pulsed stimulated infrared thermography applied to carbon-epoxy non destructive evaluation', Proc. of QIRT 92, pp 195-199, July 1992.
12. E Grinzato and V Vavilov, 'Corrosion evaluation by thermal image processing and 3D modelling', Rev. gén. Therm., Vol 37, pp 669-679, 1998.
13. M Krishnapillai et al., 'Thermography as a tool for damage assessment', Composite Structures, Vol 67, pp 149-155, 2005.
14. M Krishnapillai et al., 'NDTE using pulse thermography: Numerical modelling of composite subsurface defects', Composite Structures, Vol 75, pp 241-249, 2006